

Simultaneous Measurements of Electrostatic and Magnetic Fluctuations in ASDEX Upgrade Edge Plasma

Codrina Ionita¹, Nicola Vianello², Hans W. Müller³, Franz Mehlmann¹, Matteo Zuin², Volker Naulin⁴, Jens J. Rasmussen⁴, Volker Rohde³, Roberto Cavazzana², Catalin Lupu¹, Marc Maraschek³, Roman W. Schrittwieser¹, Petru C. Balan¹, ASDEX Upgrade Team³

¹Association EURATOM/ÖAW, Institute for Ion Physics and Applied Physics, University of Innsbruck, Austria

²Association EURATOM/ENEA, Consorzio RFX, Padova, Italy

³Association EURATOM/IPP, Max-Planck-Institute for Plasma Physics, Garching, Germany

⁴Association EURATOM/RISØ-Technical University of Denmark, Roskilde, Denmark

(Received: 5 September 2008 / Accepted: 18 February 2009)

In ASDEX Upgrade (AUG) electrostatic and magnetic fluctuations in the edge plasma region were measured simultaneously during ELMy H-mode (high confinement) plasmas and L-mode (low confinement) plasmas and during a transition between the two modes. A special probe was used containing six Langmuir probe pins of graphite of which one is protruding radially. In addition, 20 mm behind the front side a triple magnetic pick-up coil is mounted inside the probe head by which temporal variations of the magnetic field in all three directions of space can be detected. The probe pins are arranged in such a way that simultaneously the poloidal and radial electric field components, the ion saturation current and the current-voltage characteristic can be registered. During the AUG discharges of 7 s lengths the probe head is inserted two to three times for 100 ms each by the midplane manipulator into the scrape-off layer outside the last closed flux surface. The main emphasis is put on type I ELMs and from the results the radial turbulent particle flux and magnetic field variations are determined.

Keywords: edge plasma turbulence, edge localized modes, electrostatic fluctuations, magnetic fluctuations, turbulent flux.

1. Introduction

Edge localized modes (ELMs) are short breakdowns of the high confinement regime (H-mode) in large and mid-sized tokamaks [1]. There are several types of ELMs of which type I ELMs are the strongest events. In ASDEX Upgrade (AUG) type I ELMs have typical durations of a few ms, occurring at more or less regular intervals with typical repetition frequencies of around 100 Hz once the plasma pressure exceeds a critical value in the edge transport barrier region. Rapid loss of energy and particles and the associated high power fluxes from the confined region into the scrape-off layer (SOL) will lead to unacceptable high local power loads on plasma facing components for a power producing magnetic confinement fusion device such as ITER and future fusion reactors [2]. Understanding and controlling ELM events and their power deposition is therefore one of the foremost priorities in fusion research.

At present ELMs are thought to originate from a combination of current and pressure gradient driven MHD modes [3]. ELMs result in intermediate mode number ($n \approx 10-15$) structures [4,5,6,7], which are well localized perpendicular to the magnetic field and extend parallel to it. These filaments propagate through the SOL, where they

have been measured using Langmuir probes on various machines [8,9,10,11,12]. Magnetic fluctuations associated with ELMs are usually ascribed to MHD activity. In the past they were measured mainly by magnetic pickup coils close to the vessel wall [6,13] with the exception of [4,10,12] where also magnetic coils in the probe head were used. Measurements taking place far from the filaments in comparison to the radial extent of these structures make it difficult to observe the magnetic perturbation going along with individual filaments and to examine the magnetic fine structure of the ELMs. Both would result in important information to complete the dynamical picture of ELMs and their underlying instability, such as the excursion of magnetic field lines from their equilibrium position, and the question whether or not ELMs are associated with reconnection events [14].

In this contribution we present results on simultaneous investigations of electric and magnetic fluctuations in AUG SOL plasma by means of a probe head combining Langmuir probes and magnetic pick-up coils, mounted on the mid-plane manipulator. Thereby we have performed localized measurements of all three components of the magnetic field simultaneously with density and potential

author's e-mail: codrina.ionita@uibk.ac.at

fluctuations at close distance from each other. This elucidates the penetration of ELM filament structures into the SOL. Our measurements allow indicating the presence of current filaments associated with ELMs thus opening a new window on their characterization.

2. The probe head

2.1. Electric probes

Fig. 1 shows a schematic drawing of the probe head. On the front side of a cylindrical graphite case of about 60 mm diameter and 150 mm length six graphite pins of 1 mm diameter and 2 mm length are mounted isolated from each other by boron nitride, which is retracted to avoid damages by the radiation from the plasma. The six pins are arranged in two rows of three pins each with a distance of 10 mm from each other. In poloidal direction the two rows of pins are situated above each other with a distance of 10 mm in between. The numbering of the probes is indicated in the insert, which shows the probe arrangement as seen from the plasma. The leftmost upper pin (probe 1) protrudes by 3 mm from the plane of the other five pins. Probe 1, 2, 3 and 6 serve to measure the floating potentials $V_{fl,1-3,6}$, and $d_{12} = 3$ mm is thus the radial distance between probes 1 and 2, while $d_{36} = 10$ mm is the poloidal distance between probes 3 and 6. Probe 4 is negatively biased to record the ion saturation I_{is} from which the ion density can be derived. Probe 5 is swept to register the current-voltage characteristic from which the electron temperature T_e can be deduced in the usual way. The probe measurements have an upper cut-off frequency of about 100 kHz.

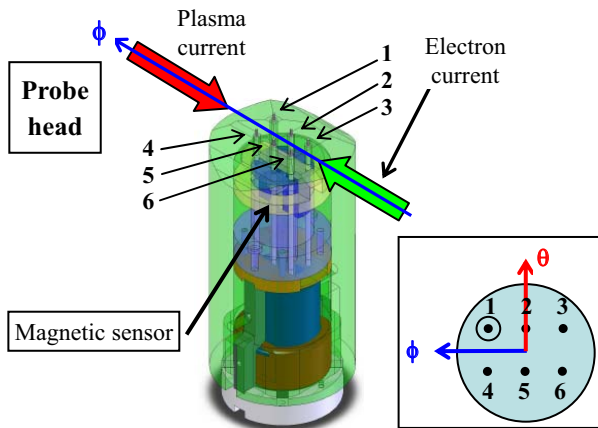


Fig. 1. Schematic drawing of the probe head. The probe pins are numbered with probe 1 protruding by 3 mm from the other probes. In the toroidal and poloidal directions the distance between the probe pins is 10 mm, respectively. The insert shows the front side of the probe head as seen from the plasma.

With this probe arrangement both, the poloidal and the radial electric field component can be determined by:

$$E_\theta = \frac{V_{fl,6} - V_{fl,3}}{d_{36}} \quad E_r = \frac{V_{fl,2} - V_{fl,1}}{d_{12}} \quad (1)$$

But we have to be aware that these formulae only yield approximate results. First the deduction of the electric field is limited to potential variations that are large compared to the probe separation and in addition one has to take into account the integrating over space properties of the probe pins. Furthermore we only measure the cold floating potentials

$$V_{fl} = \Phi_{pl} - \alpha \frac{T_e}{e}, \quad (2)$$

which still contain the electron temperature, whereas the true value of the plasma potential Φ_{pl} does not depend on T_e [15]. Thus in principle we have to assume that the electron temperature, and in particular its fluctuations, are identical on both respective probe positions (3 and 6 on one side and 1 and 2 on the other side). However, if there are temperature fluctuations we would expect that they have a similar spatial scale as density and potential. Therefore it suffices to assume that T_e -fluctuations are small and close to, or in phase with the density fluctuations [16]. One should note that within the ELM filaments the assumption of small temperature fluctuations is potentially violated leading to larger measurement errors during ELM phases. In this context we would like to point out that a more reliable measurement of the electric field components can be achieved by emissive probes whose floating potential is closer to the true value of Φ_{pl} than V_{fl} [16]. However, in ASDEX Upgrade the use of emissive probes was not yet attempted.

In Eq. (2) $\alpha = \ln(I_{es}/I_{is})$ is the ratio of electron to ion saturation current to the probe. In the edge region of a toroidal plasma α is typically 2 [17] depending not only on the electron temperature, but also on the effective collecting probe areas $A_{ep,ip}$ for electrons and ions, respectively, which can differ in a strong magnetic field.

The ion saturation current measured with probe 4 allows the approximate determination of the plasma density:

$$n_{pl} \cong n_i = \frac{I_{is}}{eA_{ip}} \sqrt{\frac{m_i}{T_e}}. \quad (3)$$

Here m_i is the ion mass. This formula is derived under the assumption that at the probe sheath edge the Bohm criterion is fulfilled. Also in this case we have to take into account that the unknown fluctuations of T_e can have a decisive influence on the determination of the ion density fluctuations. According to Ref. 16 the influence of \tilde{T}_e on \tilde{n}_{pl} is even stronger than on \tilde{E}_θ or \tilde{E}_r .

Knowing \tilde{E}_θ and \tilde{n}_{pl} we can deduce the radial fluctuation-induced particle flux (or simply "turbulent flux") [18]

$$\Gamma_r = \langle \tilde{n}_{pl} \tilde{v}_r \rangle = \frac{\langle \tilde{n}_{pl} \tilde{E}_\theta \rangle}{B_\phi} \quad (4)$$

with B_ϕ being the toroidal magnetic field which here serves as an approximation for the total magnetic field B . The radial drift velocity v_r is here approximated by the $E_\theta \times B$ particle drift. In principle also the Reynolds stress can be determined with this probe array, but this will be subject of a later paper.

2.2. Magnetic pick-up coils

Inside the graphite case, 20 mm behind the front side, a magnetic sensor is mounted by which the time derivative of the three components of the magnetic field are measured. The sensor consists of three coils produced by winding a 0.2 mm diameter wire around a small parallelepiped-shaped support of Vespel of $7 \times 7 \times 8 \text{ mm}^3$ dimensions.

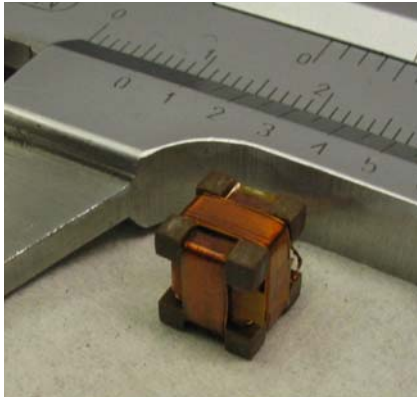


Fig. 2 Photo of the magnetic sensor with scale.

Fig. 2 shows a photo of the magnetic sensor. The bandwidth for magnetic measurements is above 1 MHz with -3 dB cutoff at 1.1 MHz [19].

The probe head shown in Fig. 1 was mounted on the midplane manipulator of AUG and inserted during the AUG discharges of about 7 s length two or three times into the SOL up to a about 5 cm in front of the last closed flux surface, where the standstill time was about 100 ms on a constant radial position.

3. Experimental results

3.1. Global plasma parameters

In the following we present selected results from three different discharges whose global parameters are listed in Table I. Shot #23157 is an L-mode plasma, whereas shot #23161 is an H-mode plasma. The results of shot #22748 show a transition from the H-mode to the L-mode towards the end of the discharge.

3.2. Electric probe measurements

As an example we first show the current-voltage characteristic $I_p(V_p)$ of probe 5 during L-mode shot #23157 from which we have determined the electron temperature in the SOL as 6.5 eV (Fig. 3). As shown in Table I this is a purely Ohmic plasma with relatively low density.

Table I: Global parameters of the discharges evaluated

Shot number	I_p (MA)	n_e (m^{-3})	B_t (T)	q_{95}	P_{NBI} (MW)	$P_{heat,total}$ (MW)
#22748 (H \Rightarrow L-mode)	0.800	6.9×10^{19}	-2.472	5.237	2.623	4.007
#23157 (L-mode)	0.801	4.92×10^{19}	-2.476	5.260	0	0.7
#23161 (H-mode)	0.800	6.77×10^{19}	-2.477	5.226	5.139	8.660

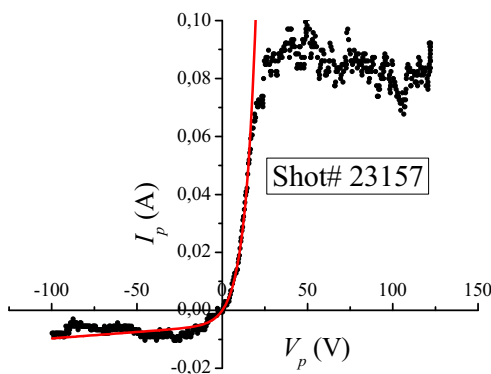


Fig. 3. Current voltage characteristic of probe 5 in the SOL: the red line shows the fitted characteristic.

We see that both, the magnitude of the ion saturation current and that of the electron saturation current appear to decrease for more negative or positive probe voltages, respectively. This is not a typical effect, but needs further investigation. On the other hand, the range from which T_e was determined is not affected, and in both cases for $|V_p| > 100 \text{ V}$ approximately, both the magnitudes increase again.

The main goal of the electrostatic probe measurements was the determination of the turbulent flux (Eq. 4) in various discharges and in particular during type-I ELMs and during the quiet time in between ELMs. The former will be called "ELMs intervals", the latter "inter-EML intervals".

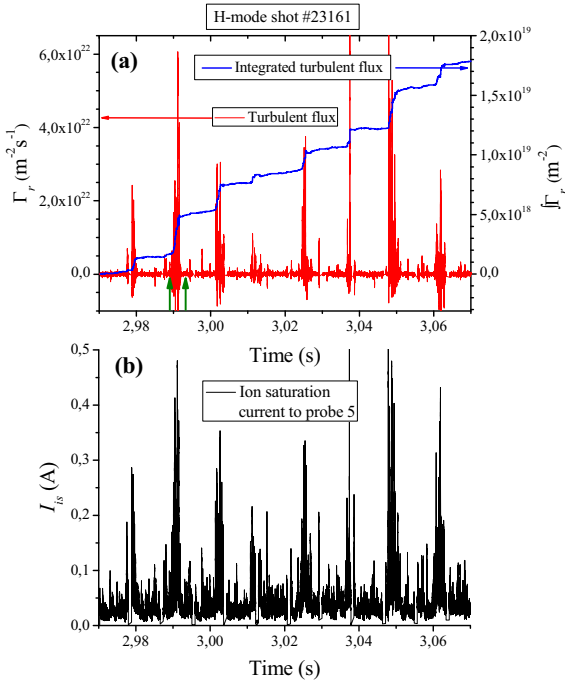


Fig. 4. Temporal evolution during the entire probe insertion: (a) instantaneous radial turbulent flux (red) and its integral (blue) showing type I ELMs, (b) ion saturation current to probe 4 during the same interval. The two green arrows indicate the detail shown in Fig. 5.

Fig. 4(a) shows for H-mode shot #23161 the instantaneous radial turbulent flux $\Gamma_{r,inst} = (n_{pl}E_{\theta})/B_{\phi}$ in red and its integral $\int_0^t \Gamma_r dt' = \left(\int_0^t n_{pl}E_{\theta} dt' \right) / B_{\phi}$ in blue with $t_0 = 2.97$ s. The latter shows the temporal increase of the radially transported particles. In Fig. 4(a) the ELMs are well visible during the observation interval $2.97 \leq t \leq 3.07$ s as eight strong intermittent fluctuation events (red line) with a repetition rate of about 12 ms.

The integrated flux (blue line) gives insight into the turbulent transport during ELM intervals (steep stepwise increases) and inter-ELM intervals (flat portions), and the averaged flux Γ_r is given by the steepness of the steps and flat parts, respectively.

Fig. 4(b) shows the ion saturation current I_{is} to probe 4 during the same interval. Also in this case the ELMs are easily discernible by the sudden increases of I_{is} , which are indications of sudden density increases. The ELM bursts in I_{is} have a qualitatively similar structure as those in Fig. 4(a) of the flux and the integrated flux.

Fig. 5(a) shows the second ELM event in the extended interval $2.989 \leq t \leq 2.993$ s. This interval is marked by two vertical green arrows in Fig. 4(a). From both, the instantaneous flux and the integrated one, we see that the ELM has a fine structure, which is in qualitative agreement with previous measurements [8] and supports the filamentary model of type-I ELMs [4].

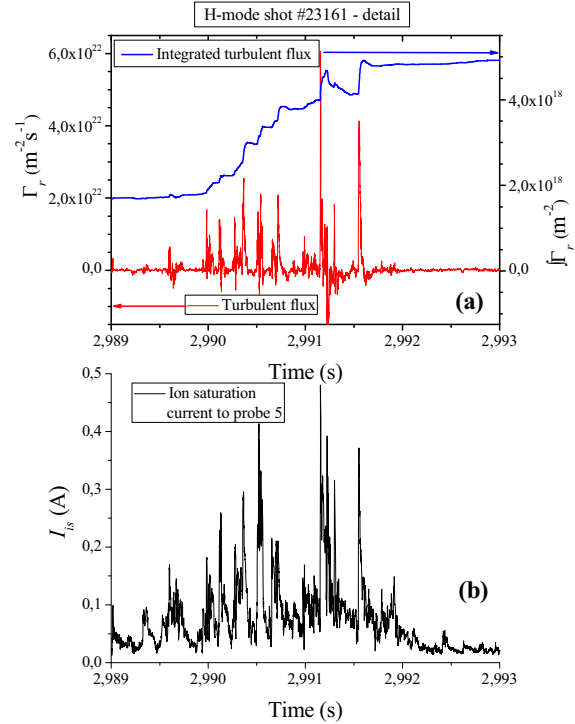


Fig. 5. Detail of temporal evolution of Fig. 4 during the interval indicated by two green arrows in Fig. 4(a).

From Fig. 5(a) we see also that there are strong negative transport events during an ELM: around $t = 2.99123$ s we observe a deep minimum of Γ_r . Also the integral of the flux (blue line) has a negative slope in the range $2.99121 \leq t \leq 2.99154$ s, which is also an indicator of inward transport. We point out that this strong negative transport event follows right after the strongest positive transport event for $t = 2.99115$ s. This pattern is similar for all ELM fine structure filaments.

There is also a qualitative similarity of the ELM filaments in the flux and the integrated one with the ELM bursts in I_{is} but the similarity is less striking than in Fig. 4(a,b).

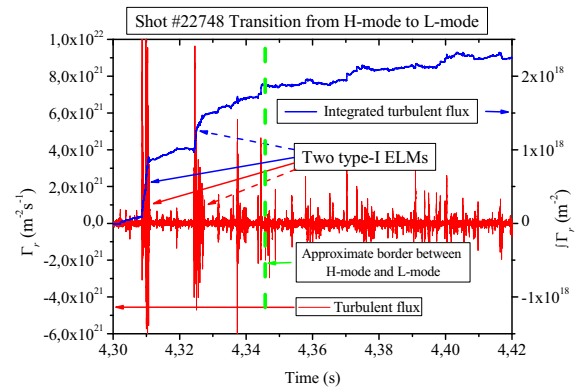


Fig. 6. Instantaneous radial turbulent flux (red) and its integral (blue) showing a transition from the H-mode to the L-mode. The approximate transition time between the two modes is indicated by a vertical green dashed line.

Fig. 6 shows the instantaneous and integrated flux during the last insertion of the probe head into the SOL during shot #22748. During this insertion we were fortunate to capture a transition from the H-mode to the L-mode towards the end of the discharge. We see two type I ELMs at the beginning of the probe insertion with two strong and steep steps of the integrated flux at about 4.309 s and 4.325 s. The transition from the H-mode appears to be rather smooth occurring somewhere around $t = 4.345$ s, indicated by a vertical green dashed line.

3.3. Magnetic measurements

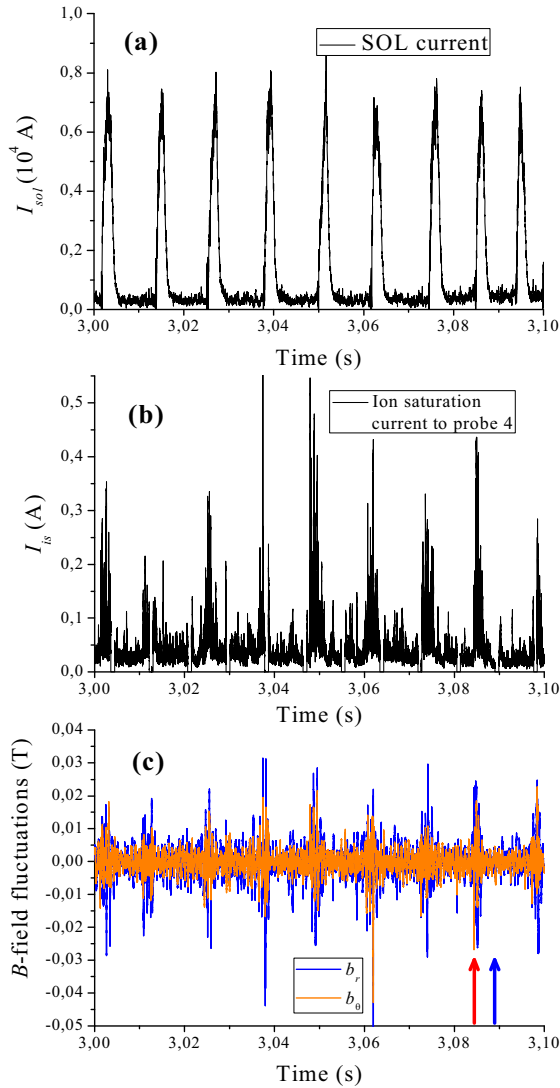


Fig. 7. Temporal evolution of shot #23161 during almost the same time window as Fig. 4: (a) current in the SOL, (b) Ion saturation current (same as in Fig. 4), (c) magnetic signals b_r and b_θ from the radial and poloidal sensor coils, respectively. The red and blue arrow in (c) show the time intervals for the hodograms in the corresponding colors in Fig. 8. In case of the red arrow the interval has a length of 0.5 ms, in case of the blue arrow 0.4 ms.

For the same shot #23161, in Fig. 7(a) we show the total current in the SOL, I_{sol} [20]. This is obtained by extrapolation of the currents to the divertor tiles. In panel (b) the locally measured ion saturation current, I_{is} , to probe 4 is depicted and in panel (c) the magnetic field fluctuations in radial and poloidal direction, b_r and b_θ , respectively, obtained by integrating the signals of the localized magnetic pickup coils. The magnetic field fluctuations are due to the corresponding variations of the current pattern in the plasma edge region.

Also in this case (Fig. 7(c)) we discern the ELMs since every ELM is thought to correspond to magnetic field aligned filaments, which mainly move radially and poloidally. At the same time they expand along the magnetic field [14].

We see that the maximum amplitude of the magnetic field perturbations is around 0.04 T. With a toroidal magnetic field strength of about 2.5 T (see Table I) this yields a relative amplitude of 0.02. This is a relatively small value. It means that on a length of 1 m a field line is deviated by less than 1 cm.

By drawing b_θ versus b_r we obtain trajectories in time, so-called hodograms, of the magnetic field fluctuations as seen in Fig. 8. These were taken in the two time intervals indicated in Fig. 7(c) by a red arrow (the interval is 0.5 ms long) and blue arrow (0.4 ms), respectively. The hodograms in the same colors refer to the two respective intervals.

The closed loop in the hodogram of Fig 8 (red curve) is a possible indication of a current filament aligned mainly in the toroidal direction associated with an ELM, whereas the blue curve in Fig. 8 shows a more complex pattern in between ELMs without closed loop [14]. From the red time interval of Fig. 8 we see that currents aligned in the toroidal direction form mainly during the growing phase of an ELM (cf. Fig. 7c).

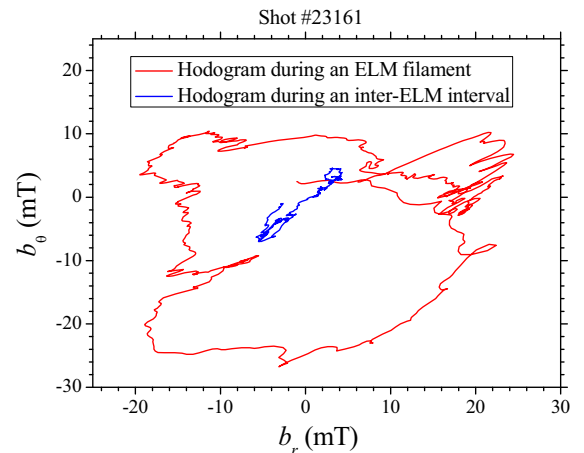


Fig. 8. Hodograms of the poloidal and radial magnetic signals, b_θ and b_r for the time intervals indicated by the arrows in the corresponding colors in Fig. 7(c): red line during an ELM interval, blue line during an inter-ELM interval.

4. Conclusion

We have used a probe system consisting of six Langmuir probes and one magnetic sensor for all three directions of space. We have investigated about eight type-I ELM events during an H-mode plasma in ASDEX Upgrade and have evaluated the instantaneous and the integrated turbulent flux associated with the ELMs. We found evidence for a filamentary structure of an ELM which typically consists of a few current filaments up to around 10. From the magnetic signals we could construct hodograms as further evidence for current filaments aligned with the magnetic field. Also the current in the filaments, producing magnetic field perturbations, are along the field lines, whereas the filament as such propagates across the field line, having mainly a radial and poloidal propagation direction.

5. Acknowledgement

This work, supported by the European Communities under the contract of Associations between EURATOM and the Austrian Academy of Sciences, the Max-Planck-Institute for Plasma Physics, Garching, ENEA/RFX, Padova, and Risø/Danish Technical University was carried out within the framework of the European Fusion Development Agreement. The content of the publication is the sole responsibility of its author(s) and it does not necessarily represent the views of the Commission or its services. This work was also supported by project L302-N02 of the Austrian Science Fund and the Excellentia Programme for graduated women of the University of Innsbruck.

6. References

- [1] See for instance: H. Zohm, *Plasma Phys. Control. Fusion* **38**, 105, (1996); D.N. Hill, *J. Nucl. Mater.* **241-243**, 182 (1997); W. Fundamenski, V. Naulin, T. Neukirch, O.E. Garcia, J. Juul Rasmussen, *Plasma Phys. Control. Fusion* **49**, R43 (2007).
- [2] G. Federici, A. Loarte, G. Strohmayer, *Plasma Phys. Control. Fusion* **45**, 1523 (2003).
- [3] P. Snyder, H. Wilson, X. Xu, *Phys. Plasmas* **12**, 056115 (2005).
- [4] A. Kirk, N. Ben Ayed, G. Counsell, B. Dudson, T. Eich, A. Herrmann, B. Koch, R. Martin, A. Meakins, S. Saarelma, R. Scannell, S. Tallents, M. Walsh, H.R. Wilson, MAST team, *Plasma Phys. Contr. Fusion* **48**, B433 (2006).
- [5] M.E. Fenstermacher, T.H. Osborne, A.W. Leonard, P.B. Snyder, D.M. Thomas, J.A. Boedo, T.A. Casper, R.J. Groebner, M. Groth, M.A.H. Kempnaars, A. Loarte, G.R. McKee, W.M. Meyer, G. Saibene, M.A. VanZeeland, X.Q. Xu, L. Zeng, DIII-D Team, *Nucl. Fusion* **45**, 1493 (2005).
- [6] A. Herrmann, A. Kirk, A. Schmid, B. Koch, M. Laux, M. Maraschek, H.W. Mueller, J. Neuhauser, V. Rohde, M. Tsalas, E. Wolfrum, ASDEX Upgrade Team, *J. Nucl. Mat.* **363**, 528 (2007).
- [7] A. Kirk, B. Koch, R. Scannell, H. R. Wilson, G. Counsell, J. Dowling, A. Herrmann, R. Martin, M. Walsh, *Phys. Rev. Lett.* **96**, 185001 (2006).
- [8] M. Endler, I. Garcia-Cortès, C. Hidalgo, G.F. Matthews, ASDEX Team, JET Team, *Plasma Phys. Control. Fusion* **47**, 219 (2005).
- [9] see e.g.: A.W. Leonard, N. Asakura, J.A. Boedo, M. Becoulet, G.F. Counsell, T. Eich, W. Fundamenski, A. Herrmann, L.D. Horton, Y. Kamada, A. Kirk, B. Kurzan, A. Loarte, J. Neuhauser, I. Nunes, N. Oyama, R.A. Pitts, G. Saibene, C. Silva, P.B. Snyder, H. Urano, M.R. Wade, H.R. Wilson, the Pedestal and Edge Physics ITPA Topical Group, *Plasma Phys. Contr. Fusion* **48**, A149 (2006).
- [10] A. Schmid, PhD thesis, Technical University of Munich (2008), <http://edoc.mpg.de/display/epl?mode=doc&id=359520&col=33&grp=1311#cb>
- [11] J. Neuhauser, V. Bobkov, G.D. Conway, R. Dux, T. Eich, M. Garcia-Munoz, A. Herrmann, L.D. Horton, A. Kaltenbach, S. Kalvin1, G. Kocsis, B. Kurzan, P.T. Lang, M. Maraschek, H.W. Mueller, H.D. Murmann, R. Neu, A.G. Peeters, M. Reich, V. Rohde, A. Schmid, W. Suttrop, M. Tsalas, E. Wolfrum, ASDEX Upgrade Team, *Nucl. Fusion* **48**, 045005 (2008).
- [12] A. Herrmann, A. Schmid, H.W. Müller, M. Maraschek, J. Neuhauser, A. Kirk1, ASDEX Upgrade Team, 22nd IAEA Fusion Energy Conference (Geneva, Switzerland, 13-18 October 2008), IAEA-CN-165/ EX/P6-1.
- [13] H. Takahashi, E.D. Fredrickson, M.J. Schaffer, *Phys. Rev. Lett.* **100**, 205001 (2008).
- [14] W. Fundamenski, V. Naulin, T. Neukirch, O.E. Garcia, J. Juul Rasmussen, *Plasma Phys. Contr. Fusion* **49**, R43 (2007).
- [15] I.H. Hutchinson, *Principles of Plasma Diagnostics* (Cambridge University Press, Cambridge, 1987), p. 64.
- [16] R. Schrittwieser, C. Ionita, P. Balan, C. Silva, H. Figueiredo, C.A.F. Varandas, J. Juul Rasmussen, V. Naulin, *Plasma Phys. Contr. Fusion* **50**, 055004 (2008).
- [17] R. Schrittwieser, J. Adamek, P. Balan, M. Hron, C. Ionita, K. Jakubka, L. Kryska, E. Martines, J. Stöckel, M. Tichy, G. Van Oost, *Plasma Phys. Control. Fusion* **44**, 567 (2002).
- [18] E.J. Powers, *Nucl. Fus.* **14**, 749 (1974).
- [19] N. Vianello, V. Antoni, E. Spada, M. Spolaore, G. Seriani, R. Cavazzana, H. Bergsaker, M. Cecconello, J.R. Drake, *Nucl. Fusion* **45**, 761 (2005).
- [20] A. Kallenbach, A. Carlson, G. Pautasso, A. Peeters, U. Seidel, *J. Nucl. Mat.* **290-293**, 639 (2001).